Numerical Simulation of TwoDimensional Turbulence

Douglas K. Lilly

Citation: Phys. Fluids **12**, II-240 (1969); doi: 10.1063/1.1692444
View online: http://dx.doi.org/10.1063/1.1692444
View Table of Contents: http://pof.aip.org/resource/1/PFLDAS/v12/i12
Published by the AIP Publishing LLC.

Numerical Simulation of Two-Dimensional Turbulence

DOUGLAS K. LILLY
National Center for Atmospheric Research, Boulder, Colorado

The two-dimensional incompressible Navier–Stokes equations are numerically integrated in order to test the validity of Kraichnan's predictions on the structure of two-dimensional turbulence. The numerically simulated turbulence is produced by an artificial forcing function, constructed from a randomly varying set of Fourier modes lying within a narrow spectral band near scalar wavenumber k_e. For the case of turbulence maintained by a constant rate of energy injection, Kraichnan predicts the development of two power-law energy spectra, a $k^{-5/3}$ range for frequencies less than k_e, and a k^{-3} range for those greater than k_e. The numerical results are consistent with these predictions, although truncation and aliasing errors restrict the useful spectral range of the calculations to less than that desirable for a fully satisfactory test. The predictions and results are apparently relevant to several areas of geophysical fluid dynamics and to the correct interpretation of other numerical simulation experiments.

I. INTRODUCTION

The principal computations reported in this paper were intended to test the validity of Kraichnan's predictions on the character of the two-dimensional turbulence produced by random, nearly monochromatic, constant amplitude forcing.[1] The model deduced by Kraichnan, if valid, appears to have application to various kinds of quasi-two-dimensional turbulence in geophysical fluid dynamics. The calculated results also provide a somewhat stringent test of the adequacy of the numerical procedures used to obtain them.

II. KRAICHNAN'S HYPOTHESIS

It has long been noted that the assumptions leading to the Kolmogoroff energy spectrum in the inertial range of turbulent flow are not formally restricted to three-dimensional flow, although the validity of the Kolmogoroff spectrum apparently is. It has also long been noted that two-dimensional inviscid flow contains, in addition to kinetic energy, a second quadratic invariant, the squared vorticity, which is by definition twice the enstrophy.[2] In the viscous case, therefore, two kinds of dissipation may be considered fundamental: that of kinetic energy ϵ and that of enstrophy η. Correspondingly, Kraichnan noted that two kinds of inertial ranges could formally be defined: that of Kolmogoroff in which energy is transferred through wavenumber space, and a new one in which enstrophy is similarly transferred. The first leads, of course, to the familiar and experimentally rather well-verified (in three-dimensional turbulence) $k^{-5/3}$ power law for the scalar energy, spectrum of scalar wavenumber k; while the second, by similar dimensional reasoning, leads to a k^{-3} law. Kraichnan was also able to prove that these transfers are mutually exclusive; thus, a $k^{-5/3}$ spectrum cannot transfer enstrophy up or down scale, and similarly energy cannot be propagated in wave space through a k^{-3} region. A similar proof was produced by Leith[3] within the context of a simplified closure approximation for the energy spectrum equation.

We now consider a hypothetical physical situation. A random forcing disturbance consisting of components chosen from a narrow region of spectral space in the neighborhood of scalar wavenumber k_e, but isotropic and homogeneous, continually produces kinetic energy and enstrophy within a viscous fluid of large but finite Reynolds number (as defined in Sec. V). Kraichnan's hypothesis in a slightly modified form consists of the following prediction for the form of the developing energy spectrum

$$E(k) = \begin{cases} \alpha\left(\dfrac{d\bar{E}}{dt}\right)^{2/3} k^{-5/3}, & k_c < k < k_e; \\ \beta\eta^{2/3}k^{-3}, & k_e < k < k_d, \end{cases} \tag{1}$$

where $E(k)$ is the scalar energy spectrum of scalar wavenumber k; $\bar{E}$ is the total energy, equal to

$$\int_0^\infty E(k)\, dk;$$

k_e is the central wavenumber of the forcing disturbance; k_c and k_d are the low- and high-wavenumber limits of the spectrum; and α and β are dimensionless constants. This idealized model spectrum is depicted on a log–log plot in Fig. 1, showing its development

[1] R. Kraichnan, Phys. Fluids **10**, 1417 (1967).

[2] The term "enstrophy" for half the squared vorticity was first suggested by Nickel and has appeared in a paper by Leith (Ref. 3). It was created from the Greek root "strophe," meaning "act of turning."

[3] C. E. Leith, Phys. Fluids **11**, 671 (1968).

with time. In the high-frequency spectrum, enstrophy is transferred to higher frequencies at the enstrophy dissipation rate η, and k_d represents a dissipation length scale. Kinetic energy cannot be transferred through this range and therefore, is not dissipated, provided that $k_e \ll k_d$. Kinetic energy is, however, transferred to larger scales through the $k^{-5/3}$ spectral region, and the lower limit k_c is necessarily a decreasing function of time. Eventually, when k_c reaches the scale limit of the physical system, e.g., size of the earth or other physical boundary then energy must begin to pile up at the lowest available wavenumber.

The cutoff frequencies k_c and k_d are modeling idealizations and should not be taken as indicating sharp breaks in the spectrum. In a more complete analysis the spectrum should be considered as a generalized function of $d\bar{E}/dt$, η, k, viscosity, and time. Such an analysis additionally predicts that the low-frequency spectrum is a function of the dimensionless group $(d\bar{E}/dt)^{1/2}kt^{3/2}$, so that in the present approximation $k_c \propto (d\bar{E}/dt)^{-1/2}t^{-3/2}$.

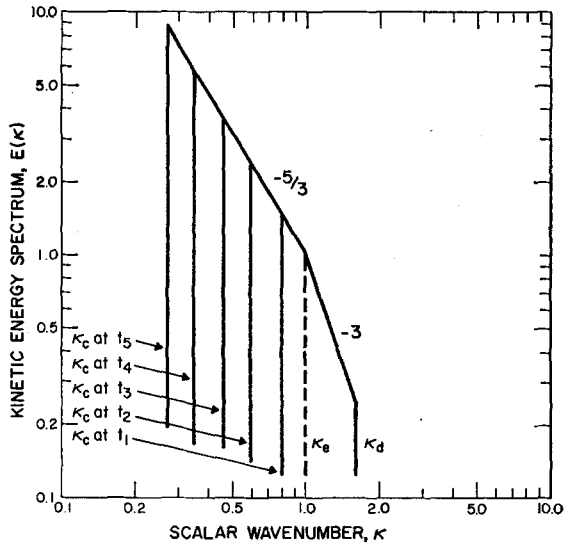

FIG. 1. Schematic scalar energy spectrum for forced two-dimensional turbulence as predicted by Kraichnan and interpreted in this paper. Energy is injected or generated in the vicinity of scalar wavenumber k_e and is transferred to lower frequencies through a growing $k^{-5/3}$ range, with a moving lower limit k_c. Mean-squared vorticity (enstrophy), also produced at k_e, is transferred to higher frequencies through a k^{-3} range terminating at a dissipation scale k_d. Ideally (though not on this depiction) $k_c \ll k_e \ll k_d$.

III. THE NUMERICAL MODEL

The appropriate differential equations for simulation of the situation envisioned by Kraichnan are the following:

$$\frac{\partial \zeta}{\partial t} + \mathbf{V}\cdot\nabla\zeta = F + \nu\nabla^2\zeta, \tag{2}$$

$$\mathbf{V} = -\mathbf{i}\frac{\partial \psi}{\partial y} + \mathbf{j}\frac{\partial \psi}{\partial x}, \qquad \zeta = \nabla^2\psi, \tag{3}$$

where ζ is the component of vorticity perpendicular to the x-y plane of the motion field, equal to the two-dimensional Laplacian of a stream function ψ. $F(x, y, t)$ is the forcing function (actually the curl of an applied force per unit mass), and ν is the kinematic viscosity. The boundary conditions are chosen to be cyclic in both x and y directions, so that the motion is periodic with a wavelength equal to the dimension of a square. Initially, the motion field is zero. The numerical integration of Eqs. (2) and (3) is performed by replacing these with finite difference equations operating on variables prescribed on a Cartesian grid. The solution of the Poisson equation in Eq. (3) for ψ is performed by a fast Fourier transform method which yields exact solutions of the difference equations.

The numerical space-differencing method used on the nonlinear terms of Eq. (2) in most of these experiments is the second-order scheme developed by Arakawa,[4] which conserves kinetic energy and enstrophy within the nonlinear terms. In some experiments Arakawa's fourth-order scheme is used for comparison. The Laplacians in Eqs. (2) and (3) are approximated by the second-order expression using the center and four immediately contiguous points. Time integration is performed by the second-order Adams–Bashforth method, which is known to be slightly unstable. The time step is limited, however, to allow less than 0.1% (and in some cases 0.01%) energy amplification per time step in the inviscid, nonforced case. Probably the most serious numerical error is that associated with aliasing of the high-frequency wavenumber components in the nonlinear interactions. Although the aliasing does not lead to instability in Arakawa's difference schemes, it distorts the spectrum to some degree, particularly for wavelengths less than four times the grid distance. In the present experiments a grid mesh of 64 × 64 points is used, which allows Fourier components of up to wavenumber 32 in each direction. Components with wavenumbers greater than 16, therefore, are subject to possibly serious distortion from aliasing errors. Further details on these numerical methods and the aliasing stability problems are contained in a previous paper by this author.[5]

[4] A. Arakawa, J. Comput. Phys. 1, 119 (1966).
[5] D. K. Lilly, Monthly Weather Rev. 93, 11, (1956).

Prescription of the forcing function is obviously a critical part of the experiment. Kraichnan envisioned a constant energy and enstrophy source, but simulating this is not a simple matter since it requires a constant covariance between both ψ and F and ζ and F. It appears more straightforward to set the amplitude of F constant, but vary its phase and Fourier component structure randomly with time. Thus, F is computed from the following time difference equation:

$$F_{n+1} = R_n F_n + (1 - R_n^2)^{1/2} \hat{F}_{n+1}, \tag{4}$$

where the subscript for F refers to the time-step level, R_n is a dimensionless correlation coefficient ≤ 1, and $\hat{F}_n$ is a randomly chosen part of F_n. By squaring both sides of Eq. (4) and noting that F_n and $\hat{F}_{n+1}$ are uncorrelated, it is evident that if $\overline{F_1^2} = \overline{\hat{F}_n^2}$ (the bars refer to spatial averaging), then $\overline{F_n^2}$ remains constant with time. The term $\hat{F}_n$ is obtained by randomly choosing, from a Gaussian distribution, amplitude coefficients for all the wavenumber components lying on the surface of a *square* in k_x, k_y space of width $2k_e$. Thus, all the Fourier modes having either k_x or $k_y = k_e$ are represented in $\hat{F}_n$, but with randomly variable weights. The total amplitude of $\hat{F}_n$ is controlled by normalizing the component amplitudes so that the sum of their squares is constant. The scalar energy spectra to be presented subsequently are also obtained as the sums of squared amplitude coefficients on a square of side $2k$, rather than on a circle of radius k as is usual in analytic studies.

Equation (4) defines a first-order Markov process. This particular type of forcing function probably does not exactly correspond to an easily realized physical process. We may think of it as roughly analogous to the disturbance produced by a number of stirring devices moving about slowly and randomly in the fluid. Thermal and magnetic analogies are also conceivable.

We may also write Eq. (4) as an approximation to the following differential equation:

$$\frac{\partial F}{\partial t} = -\frac{F}{\tau} + \lim_{\Delta t \to 0} \frac{\hat{F}}{(\tau\, \Delta t/2)^{1/2}}, \tag{5}$$

where

$$\frac{\tau}{\Delta t} = \frac{1}{2} \frac{1 + R_n}{1 - R_n} \tag{6}$$

and Δt is the integration time increment. The limiting process as $\Delta t \to 0$ is such that $\hat{F}$ maintains the same amplitude but is autocorrelated only for a time interval Δt. Thus, in the limit, $\partial F/\partial t$ becomes singular. Nevertheless, Eq. (5) can be formally integrated to yield

$$F(t) = \exp(-t/\tau) \cdot \left[F(0) + \int_0^t \lim_{\Delta t \to 0} \frac{\hat{F}(t')}{(\tau\, \Delta t/2)^{1/2}} \exp(t'/\tau)\, dt' \right]. \tag{7}$$

The term F is well defined, although its time derivative is singular. Hence, it may be substituted into the linearized form of Eq. (2) to produce general analytic solutions for ζ and, more usefully, the kinetic energy and enstrophy as functions of time in the linear stages of an integration. We make use of the above expression in Sec. VI.

Through Eq. (6), R_n is functionally related to τ, the decay time of F. In the numerical solution of Eq. (2) it is necessary to decrease the time step in order to maintain computational stability. However, if we choose τ to be a constant for a given experiment then, except for time truncation errors, the results will not be a function of Δt. Thus, we solve Eq. (6) for R_n,

$$R_n = \frac{1 - (\Delta t/2\tau)}{1 + (\Delta t/2\tau)} \tag{8}$$

and use this expression along with Eq. (4) to determine the forcing function. Our results are then a function of τ as well as of the magnitude of F, its wavenumber k_e, the viscosity coefficient ν, and the available modeling resolution.

We eliminate two of the parameters by an appropriate scaling. With ζ, t^{-1}, and τ^{-1} all scaled by $|F|^{1/2}$, the lengths scaled by $2\pi k_e^{-1}$, and velocities by $2\pi k_e^{-1} |F|^{1/2}$, then Eq. (2) *et seq.* are left in the same form but with ν scaled by $4\pi^2 |F|^{1/2}/k_e^2$. In the new dimensionless form, $|F| = 1$ and $k_e = 2\pi$. Solutions now become functions of ν, τ, the mesh interval as scaled by $2\pi k_e^{-1}$, and the number of mesh points. The dimensionless viscosity could be considered an inverse Reynolds number, but that notation is reserved for a related but different ratio.

IV. RESULTS OF COMPUTATIONS

Integrations were performed for two values of dimensionless ν, three values of τ (including $\tau = \infty$, the steady forcing function case), and two values of the scaled mesh interval. Some experimentation was also done with respect to the time step and the accuracy of the numerical scheme. In one case an integration was repeated with identical parameters but with the forcing function generated from a different portion of the random number sequence. This was

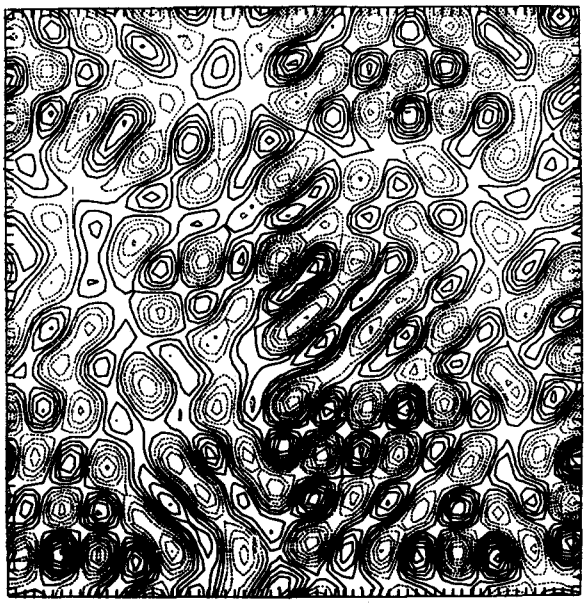

FIG. 2. A typical example of the forcing function F for a wavenumber 8 experiment. F is defined only at the intersections of the grid lines (denoted by hatch marks along the boundaries) but for easier interpretation it is machine analyzed and plotted as a continuous field.

done in order to determine whether the important statistics of a single experiment can be considered as good approximations to those of an ensemble average. (Apparently they can in that one case, at least.)

Figure 2 is a computer-analyzed map of the initial forcing function for one of the experiments. It is typical of the appearance of F at all subsequent times, although the details vary continually. The forcing function appears quasiperiodic, having 7 or 8 cycles in each direction, but with obvious larger scale modulation caused by beating between modes with frequencies the same in one direction but slightly different in the other. The mesh interval in this case is $\frac{1}{8}$ and the number of mesh points 64 in each direction, so that the components of F all have 8 waves across the square in at least one direction. Although $k_e = 2\pi$ by convention, we identify this forcing function as one of wavenumber 8.

In the early stages of a calculation both the vorticity and the stream function look very much like Fig. 2, since the development during that period is essentially linear growth of an almost monochromatic field with slight viscous damping. After 100 steps or so, depending somewhat on the parameters, nonlinear terms become dominant and rapid energy dispersion in wave space occurs. Figures 3(a) and (b) show the stream function and vorticity maps at the 160th time step for a wavenumber 8 experiment,

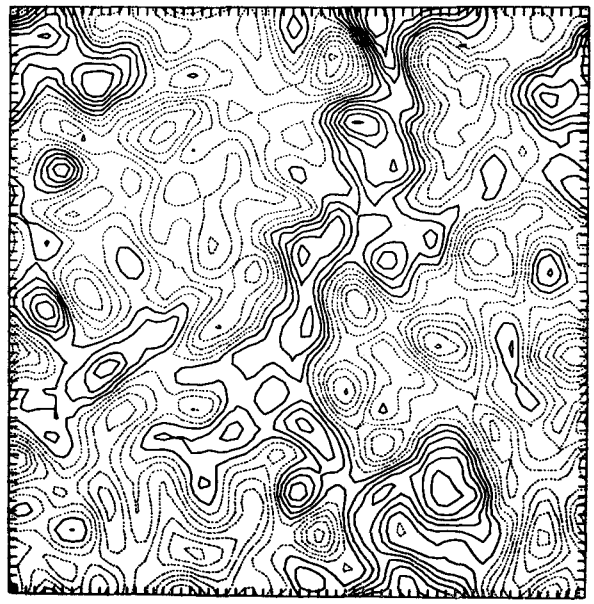

(a)

(b)

FIG. 3. Stream function (a) and vorticity (b) at the 160th time step, $t = 10.87$, for the wavenumber 8 experiment with $\nu = 2.5 \times 10^{-4}$ and $\tau = 0.5$, all in dimensionless units.

with $\tau = 0.5$, $\nu = 2.5 \times 10^{-4}$. (In the remainder of the paper we will refer to this as the basic experiment.) The vorticity field clearly exhibits a smaller scale structure than the stream field, although negative correlation between them can still be observed. At later times a high-frequency vorticity field develops in association with the shearing regions of an increasingly low-frequency stream field, which finally becomes a single dominant maximum and minimum cell pair, as shown in Figs. 4(a) and (b). Since no

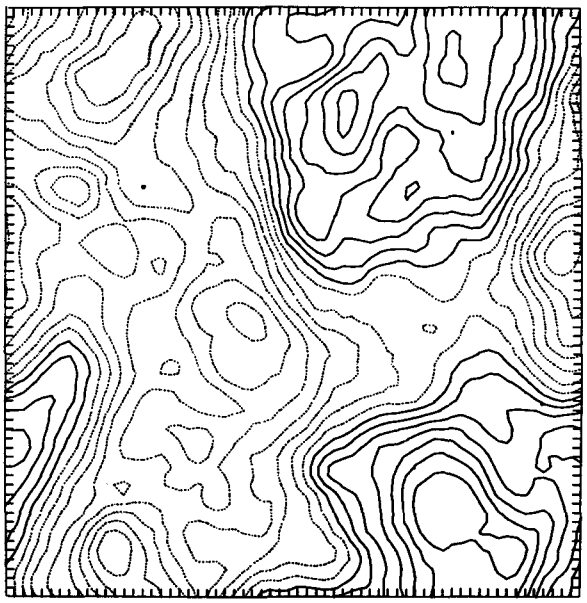

(a)

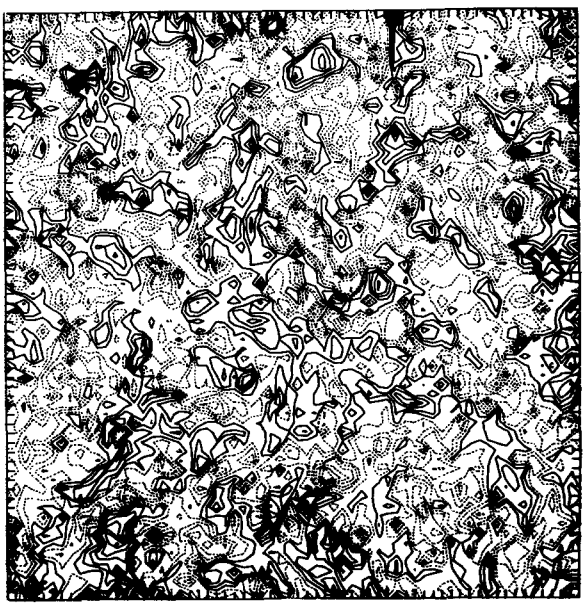

(b)

FIG. 4. Same as Fig. 3 at the 2360th step, $t = 75.45$.

mean velocity or circulation can be generated, this is about the lowest-frequency mode possible in the system, although the particular cell orientation is arbitrary and presumably random.

Figure 5 illustrates the development of the scalar energy spectrum for the basic experiment, obtained by summing up contributions around squares in wave space. Appropriate power law curves (dashed) are superimposed. The predicted development of the $k^{-5/3}$ low-frequency spectrum is apparently well verified. By 2200 time steps the entire region $k < k_e$ is saturated and is slowly piling up energy at wavenumber 1. On the other hand the high-frequency spectrum, exhibits less satisfactory verification of Kraichnan's hypothesis. The slope is evidently somewhere between $-\frac{5}{3}$ and -3; or, more likely, a -3 region exists for an octave or so, but is distorted (at the higher frequencies) by truncation or aliasing errors. There is no evidence of a viscous cutoff, although that feature did appear in experiments done with ν four times as large. The local irregularities are mostly transient, except for the sharp dip at wavenumber 32, which results because this component consists of only half as many summed terms as the others (sine terms vanish). For appropriate comparison this last point in the spectrum should have its ordinate doubled.

In order to determine which, if any, of the numerical error sources caused the apparent high-frequency discrepancy, three additional computational experiments were performed. In one, the basic experiment was restarted at the 1800th time step and run for an additional 1200 steps with the time step cut in half. This procedure effectively reduced the time truncation errors and associated high-frequency amplification by a factor of 8. In the next experiment, the same procedure was applied but Arakawa's second-order space-differencing scheme was replaced by his fourth-order method. The spatial truncation error, believed to be mainly a phase error in advection of patterns, was thereby sharply reduced. In the third additional experiment, the entire integration was repeated with the time-step criterion halved and the forcing function applied at wavenumber 4. This experiment was intended to test the effect of aliasing errors, since it allowed the enstrophy inertial range to extend to scales larger than those severely affected by aliasing. The energy spectra for the basic experiment and these three additional experiments at corresponding times are presented in Fig. 6.

By comparing the curves in Fig. 6, we see that decreasing the time-truncation error produced little if any significant change in the energy spectrum. However, decreasing the spatial trunction error by use of the fourth-order accuracy system actually increased the discrepancy between the computed spectrum and the predicted k^{-3} form. This result is consistent with the assumption that wavenumber aliasing is the major factor involved, since it can be shown that improving the accuracy of the difference scheme in this way actually increases the magnitude of the aliasing errors. The spectrum curve depicting

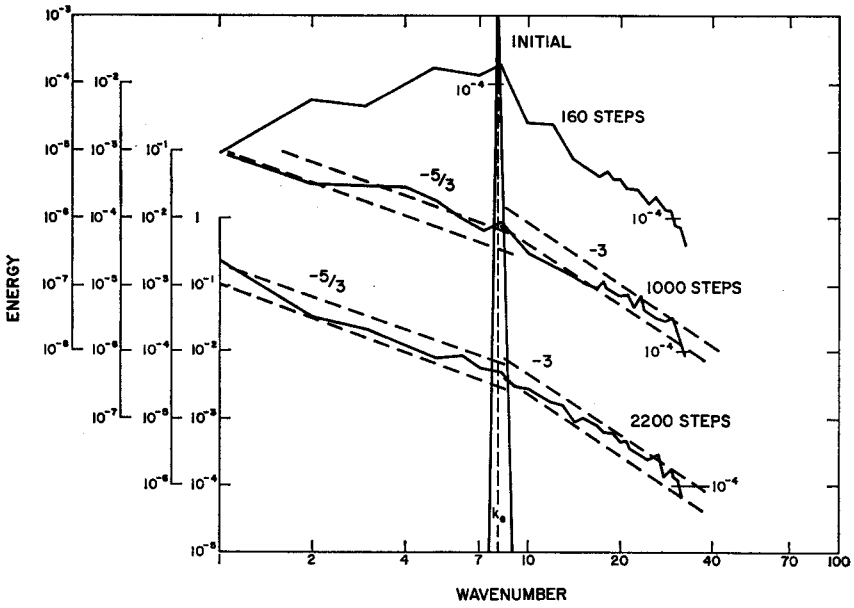

FIG. 5. The scalar energy spectrum $E(k)$ plotted on logarithmic scales at time steps 1, 160, 1000, 2200. Dashed lines with $-\frac{5}{3}$ and -3 slopes are superimposed for comparison.

the result of the third additional experiment tends to confirm this assumption: it exhibits a k^{-3} range of two octaves, from about wavenumber 4 to 16, compared with the approximate range of one octave shown in the other cases.

Figure 7 is a plot of the time dependence of three components of the scalar energy spectrum, corresponding to wavenumbers 4, 8, and 12 for the basic experiment. In the forcing component for wavenumber 8, we see the initial linear stage ending with a large overshoot, followed by a series of slowly damped oscillations apparently approaching a slowly decreasing quasiequilibrium value. The lower-frequency mode shows similar, though later and less extreme, overshooting before settling toward equilibrium. The higher-frequency mode reaches approximate equilibrium rather quickly, but is continually oscillating around it by nonlinear interactions with other modes.

In Fig. 8 the total energy and enstrophy, and the energy generation rate $-\overline{\psi F}$ are displayed as functions of time for the basic experiment. The generation rate has large temporal oscillations with somewhat greater frequency than shown, since only the results of every 40th time step were saved for the statistical analysis. These oscillations are due mainly to large variations in correlation between the forcing function and stream function components in wavenumber 8. They appear to resemble the vacillation phenomena and nonlinear oscillations observed in the large-scale circulation of the atmosphere and its experimental and computational analog. During a period of increasing correlation between $-\psi$ and F, the energy in the forcing mode also decreases rapidly. The increase is then checked by the buildup of nonlinear interactions which remove energy from that mode and tend to decouple $-\psi$ and F. This type of cyclic behavior has been investigated in a purer form by Lorenz,[6] and is apparently common (and perhaps restricted) to two-dimensional or quasi-two-dimensional fluids.

V. EVALUATION OF UNIVERSAL CONSTANTS AND FLOW PARAMETERS

Assuming that the above results may be considered sufficient to verify Kraichnan's predictions, we are now in a position to estimate the constants α and β of Eq. (1). We note first that in the case of negligible energy dissipation and constant enstrophy the the equations for the variation of energy and enstrophy are

$$\frac{d\bar{E}}{dt} = -\overline{\psi F}, \tag{9}$$

$$0 = \overline{\zeta F} - \eta. \tag{10}$$

Upon assuming continuity of the spectrum of Eq. (1) at $k = k_e$, the above expressions require that

$$\beta/\alpha = (-\overline{\psi F}/\overline{\zeta F})^{2/3} k_e^{4/3}. \tag{11}$$

If the forcing function were truly monochromatic and no truncation errors existed, then only the components with $k = k_e$ would enter into the above ratio and β would equal α. Since neither of these assumptions holds, it becomes convenient to define

[6] E. Lorenz, J. Atmos. Sci. 20, 448 (1963).

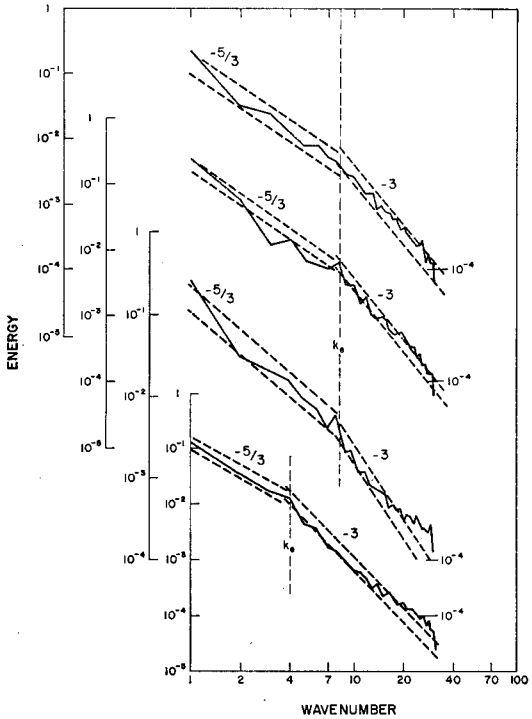

FIG. 6. Upper: Repeat of the last curve of Fig. 5. Second: $E(k)$ at 3000 time steps with the time step halved after the 1800th. Third: Same as above but with a fourth-order difference scheme used for calculation of the nonlinear terms. Lower: $E(k)$ at 2320 steps but with the forcing function assembled from wavenumber 4 components.

an effective forcing wavenumber k_{eff}:

$$-\overline{\zeta F}/\overline{\psi F} = k_{eff}^2. \tag{12}$$

By comparing the terms of the ratio for the basic experiment, we find that $k_{eff}^2/k_e^2 \sim 1.27$, which can also be predicted theoretically. If we now define α_{eff} and β_{eff} as the coefficients of Eq. (1), obtained by using k_{eff} in place of k_e, then under the conditions leading to Eqs. (9) and (10), $\alpha_{eff} = \beta_{eff}$ and both should correspond to the more idealized case of Kraichnan's model. We have evaluated α_{eff} and β_{eff} from the values of $E(k_e)$, $d\bar{E}/dt$, and η at the time corresponding to the lower curve of Fig. 5 and at $t = 20$ of the wavenumber 4 case, obtaining

$\alpha_{eff} \sim 6.2$, $\beta_{eff} \sim 4.8$, wavenumber 8;

$\alpha_{eff} \sim 4.32$, $\beta_{eff} \sim 4.05$, wavenumber 4.

The latter pair of values are probably somewhat more accurate because the wavenumber k_e is further removed from the region of severe truncation and aliasing errors.[7]

[7] Later, probably more accurate calculations of the pure decay spectrum indicate a value of β near 2.0. The discrepancy remains unexplained.

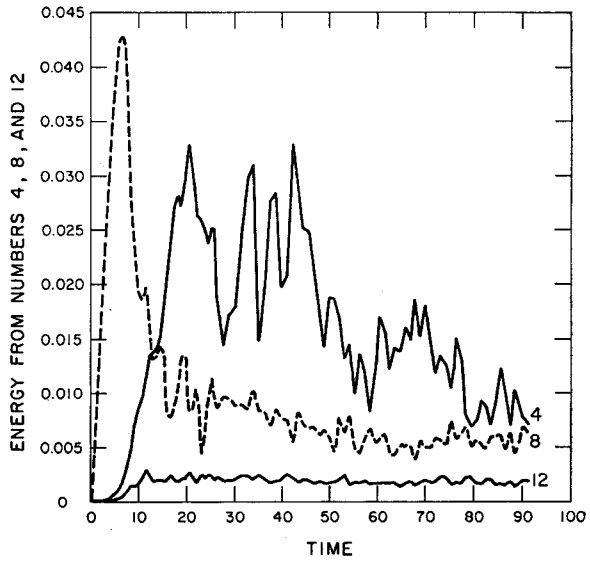

FIG. 7. Contributions to the total kinetic energy from scalar wavenumbers 4 (upper solid), 8 (dashed) and 12 (lower solid), plotted against time for the basic experiment (as illustrated in Figs. 3–5).

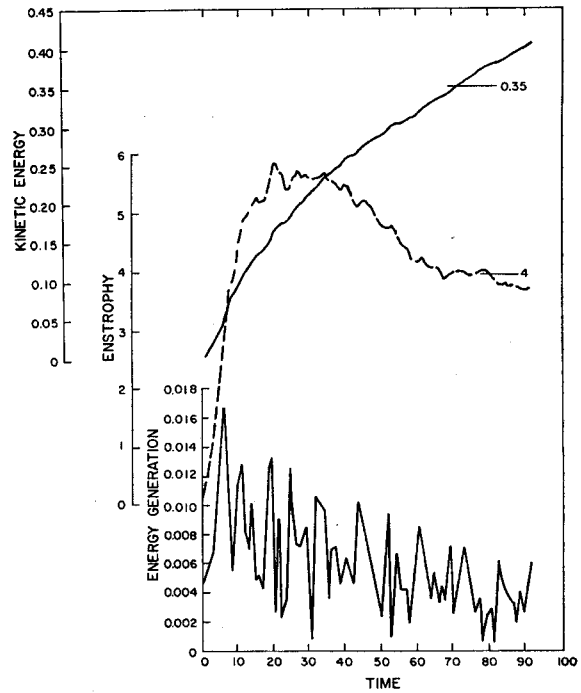

FIG. 8. Total kinetic energy, total enstrophy, and total rate of energy generation, basic experiment.

In Eq. (1) the high-frequency energy spectrum is assumed to cut off at $k = k_d$. To clarify the meaning of this we may define a nominal enstrophy dissipation scale λ_d analogous to the Kolmogoroff microscale, as

$$\lambda_d = (\nu^3/\eta)^{1/6}. \tag{13}$$

The total enstrophy dissipation can be related to the cut-off scale by evaluating the integral

$$\int_{k_c}^{k_d} k^4 E(k)\, dk$$

and equating it to $\eta/2\nu$. The result of this, after assuming that $(k_c/k_e)^{10/3} \ll 1$, is

$$\eta^{1/3}/\nu = \beta(k_d^2 - \tfrac{2}{5}k_e^2),$$

or, upon substitution of Eq. (13),

$$k_d^2 - \tfrac{2}{5}k_e^2 = 1/(\beta\lambda_d^2). \tag{14}$$

In our computations the second term on the left is almost negligible, e.g., $k_e\lambda_d \sim \frac{1}{7}$ in the basic experiment, so that $k_d\lambda_d \approx \beta^{-1/2} \sim 0.45$. Thus in the basic experiment, $k_d/k_e \sim 3$. From this result we would expect to see a viscous cutoff in the computed spectra. We attribute its absence to a combination of aliasing error in the nonlinear terms, which causes energy to pile up at high frequencies, and truncation error in the finite difference Laplacian, which decreases the viscous damping at high frequencies.

Reynolds numbers can be specified in terms of either the largest scale of motion k_c and the total rms velocity, or the forcing scale k_e and its characteristic velocity. The latter seems more relevant and is more nearly constant with time. Thus, we define R_F, the forcing Reynolds number, as

$$R_F = v_e/\nu k_e, \tag{15}$$

where

$$\frac{v_e^2}{2} = \int_{k_e}^{k_d} E(k)\, dk,$$

the energy associated with all scales smaller than the forcing scale. From the second part of Eq. (1), evaluated at k_e, we relate R_F to the enstrophy dissipation rate,

$$\eta = k_e^6\nu^3\left(\frac{R_F^3}{\beta^{3/4}}\right),$$

and upon substitution into Eqs. (13) and (14) we obtain

$$\frac{k_d}{k_e} \approx \frac{1}{\beta^{1/2}\lambda_d k_e} = \frac{R_F^{1/2}}{\beta^{3/4}}, \tag{16}$$

showing the direct connection between the forcing Reynolds number and the dissipation scale. For the basic wavenumber 8 experiment, $R_F \sim 100$; while for the wavenumber 4 case, $R_F \sim 260$.

VI. NONSTEADINESS IN THE GENERATION RATES

Somewhat unexpected behavior was observed in the time development of the energy and enstrophy integrals. The energy and enstrophy generation terms, $-\overline{\psi F}$ and $\overline{\zeta F}$, can be considered as proportional to the covariance of the forcing function amplitude and the rms velocity associated with the forcing wavenumber. That is,

$$\begin{aligned} \overline{\psi F} &= -r\,|F|\,v_F/k_{\text{eff}}, \\ \overline{\zeta F} &= r\,|F|\,v_F k_{\text{eff}}, \end{aligned} \tag{17}$$

where $v_F^2/2 = E(k_e)\Delta k$, the energy present in the forcing frequency band Δk and r is a dimensionless correlation coefficient. It has been assumed that after the initial linear stage and a period of adjustment to the nonlinear regime, r would approach a constant. In that case it could be shown that the enstrophy, the energy generation rate, and $d\bar{E}/dt$ would all become constant, as would the entire energy spectrum except for its continuing extension into lower frequencies. Figure 8 indicates that this assumption is not verified and that all the quantities expected to be constant slowly and somewhat erratically decrease. Computations made from the values of Fig. 8 show that the correlation coefficient r decreases from $\sim$0.45 at dimensionless time $t = 30$, to ~ 0.35 at $t = 90$.

The cause of this decoupling of the forcing function with the motion on the forced scale apparently lies in the development of the large-scale flow. The forcing function is locked in position and tends to produce vorticity of the same sign at a given point for the duration of its autocorrelation time τ. If a larger-scale velocity exists, say of local magnitude $\bar{U}$, it will remove the newly produced vorticity in a time of order $(k_e\bar{U})^{-1}$ and if this time is substantially shorter than τ, then the effective energy and enstrophy generation rate will diminish. A more quantitative description of the process can be derived by considering a linearized version of Eq. (2) in which the vorticity associated with the forcing scale is assumed to be a perturbation ζ' on the large-scale flow.

The linearized equation, neglecting viscosity, is

$$\frac{\partial\zeta'}{\partial t} = -\bar{U}\frac{\partial\zeta'}{\partial x} + F, \tag{18}$$

where $\bar{U}$ is a mean or large-scale velocity component. If we assume that $\zeta' \propto \exp(ik_e x)$, then Eq. (18) reduces to an ordinary differential equation, with the solution, neglecting initial conditions, given by

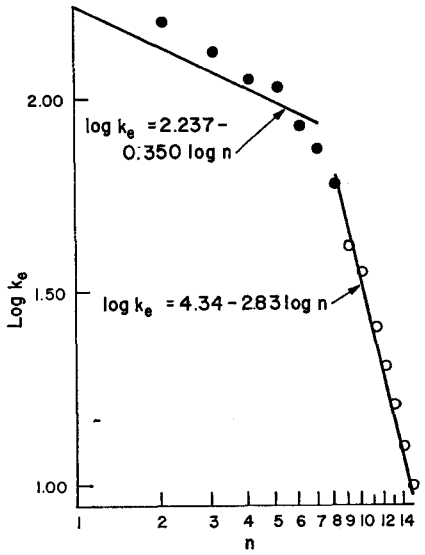

FIG. 9. Eddy kinetic energy for the total atmosphere as a function of wavenumber (from Wiin-Nielsen, Ref. 9).

$$\zeta' = \exp\,[ik_e(x - \bar{U}t)] \int_0^t \exp\,(ik_e\bar{U}s)F(s)\,ds. \quad (19)$$

The mean enstrophy production is then the real part of the integral

$$\overline{\zeta' F} = \exp\,(-ik_e\bar{U}t) \int_0^t \exp\,(ik_e\bar{U}s)\overline{F(s)F(t)}\,ds. \quad (20)$$

The term inside the integral under the bar can be evaluated by substituting Eq. (7) for $F(s)$ and $F(t)$, and performing the required integrations, recognizing that $\overline{\hat{F}(t')\hat{F}(t'')} = \overline{\hat{F}^2}$ for $|t' - t''| \leq \Delta t$ (and is zero otherwise). The result is

$$\overline{F(s)F(t)} = \overline{\hat{F}^2} \exp\,[(s - t)/\tau], \qquad s \leq t. \quad (21)$$

Upon setting this into Eq. (20) and integrating again, the real part of the enstrophy production integral is evaluated as

$$\mathrm{Re}\,(\overline{\zeta' F}) = \frac{\overline{\hat{F}^2}/\tau}{\tau^{-2} + (k_e\bar{U})^2}. \quad (22)$$

This verifies that $(k_e\bar{U})^{-1}$ is the effective coupling time when it is significantly shorter than τ. If we estimate $\bar{U}$ to be of magnitude $(2\bar{E})^{1/2}$, it becomes clear that the energy and vorticity production are considerably reduced in most of the region of integration. At the time of Fig. 4, $(k_e^2\bar{E})^{-1} \sim 30$, while $\tau^{-2} = 4$. The total enstrophy production, however, is not reduced nearly that much because in a few regions of low velocity, e.g., near the large cell centers, $\bar{U}$ is small. These regions can then dominate the spatial integral of Eq. (22). The entire effect could apparently be removed by adding an advective term $-\mathbf{V}\cdot\nabla F$ to the right side of Eq. (5) or its finite difference equivalent. In that case the forcing function would no longer be monochromatic, but it would probably correspond more accurately to typical energy-producing disturbances in real quasi-two-dimentional fluids.

VII. SOME GEOPHYSICAL AND OTHER INTERPRETATIONS

Quasi-two-dimensional flow can be produced in a laboratory under certain conditions, e.g., with strong rotation or stratification. It is a normal feature of the large-scale structure of the atmosphere and oceans of the earth, and of the atmospheres of some planets, and probably the outer layers of the sun. One of the principal qualitative effects shown in the present results, the transfer of energy from small to larger scales, has been observed and to a degree understood for many years.[8] Evidence has also been accumulating in support of the natural existence of the enstrophy inertial range. Ogura,[9] Kao and al-Gain,[10] and Wiin-Nielsen[11] have shown the apparent existence of an approximately n^{-3} energy spectrum in the atmosphere between longitudinal wavenumbers n of about 8 to at least 15. These frequencies lie in the range between those of strong baroclinic instability, where most large-scale kinetic energy is produced (4–8), and those beyond which the atmosphere can no longer be considered quasi-two-dimensional (>50).

One of Wiin-Nielsen's figures is reproduced here as Fig. 9. The low wavenumber region of is considerable interest, as it differs from the theoretical predictions and our results. In the atmosphere large-scale energy is dissipated by direct frictional contact with the ground and apparently also in regions of strong vertical wind shear near the tropopause.[12] In this respect the atmosphere differs from a two-dimensional fluid. To a first approximation, however, the effect might be simulated within the present context by adding a Hooke's law drag to the vorticity equation, thus changing Eq. (1) to

$$\frac{d\zeta}{dt} = F + \nu\nabla^2\zeta - K\zeta. \quad (23)$$

One could anticipate that if K, the surface friction coefficient, is properly scaled to correspond to the magnitude of frictional drag in the lower and upper atmosphere, its principal effect will be to remove

[8] R. Fjørtoft, Tellus 5, 225 (1953).
[9] Y. Ogura, J. Meteorol. 15, 375 (1958).
[10] S. K. Kao and A. A. al-Gain, J. Atmos. Sci. 25, 214 (1968).
[11] A. Wiin-Nielsen, Tellus 19, 540 (1967).
[12] E. C. Kung, Monthly Weather Rev. 95, 593 (1967).

energy from the most energetic parts of the spectrum, that is, from the large-scale flow.

Recent studies suggest that the solar atmosphere also is quasi-two-dimensional in its larger scales of motion.[13,14] The driving mechanism of those larger scales is unknown, but the present study suggests the possibility that the entire spectrum may be produced and maintained by energy released in the small-scale thermal convective "granulation" cells. This can only happen if the drag forces are very small. The general problem of coupling small-scale three-dimensional fluid motions in a fluid with larger, quasi-two-dimensional flow is an interesting and important one in several areas of geophysics; but it lies beyond the scope of this study.

Another area of application of the present results is in assuring a correct interpretation of two-dimensional simulations of three-dimensional fluid motions. Because of computer speed and storage limitations, most numerical solutions of flow problems have until now been restricted to two dimensions, even though in some cases the relevant physical phenomenon is known to exhibit three-dimensional turbulence. It is now clear that the only correct applications of two-dimensional numerical simulation are either to quasi-two-dimensional flows or to flows in three dimensions which are constrained, in one way or another, from becoming fully turbulent. In spite of the rapid expansion of computational facilities, simulation of fully three-dimensional flow will continue to be difficult and expensive for some time. Thus there is a need for a mathematical formulation of the equations of motion which can incorporate the *essential* effects of three-dimensionality, so far as turbulence is concerned, into a two- or "two-and-one-half-" dimensional framework.

VIII. SUMMARY

The hypothetical model of developing two-dimensional turbulence proposed by Kraichnan was tested by direct numerical integration of the Navier–Stokes equations for an incompressible viscous fluid with monochromatic but randomized forcing. The principal features predicted in the model were borne out in the computational results. In particular, results were consistent with the prediction of a $k^{-5/3}$ energy spectrum at wavenumbers less than that of the forcing function, with energy propagating to larger scales and the spectrum extending in that direction until saturated. The predicted k^{-3} region at higher wavenumbers was a little less clearly verified, apparently due to numerical problems associated with wavenumber aliasing. The attempt to diminish this problem by reducing time and space truncation errors was ineffective; but allowing the high-frequency region to extend to scales substantially larger than the 4-mesh-interval wavelength led to improvements. Nevertheless, the structure of the enstrophy inertial subrange and its transition to a viscous subrange are not yet well established.

The forcing function used in the integrations did not fully satisfy the desired constancy of energy and enstrophy injection. A partial analysis indicated that this discrepancy was associated with the lack of an advective term in the forcing function equation, which caused some decoupling with the motion fields at the forcing scale after motion fields of larger scale developed. The problem was not significant in the verification of Kraichnan's hypothesis.

The results of the calculations appear to be relevant to features of the atmosphere of the earth. In particular they may explain the k^{-3} power spectrum obtained in recent studies of the general circulation. Possible relevance to solar circulations is also suggested. Finally, the results cast doubts on the validity of attempts to simulate three-dimensional turbulence within two-dimensional computational frameworks.

ACKNOWLEDGMENTS

The computations were performed on the National Center for Atmospheric Research Control Data 6600 computer. The computer programming was handled with diligence, insight and creativity by J. Oliger and D. Fulker. The author benefited from direct discussions and correspondence with Dr. R. Kraichnan and Dr. C. E. Leith. This work was supported by the National Science Foundation.

[13] F. Ward, Pure Appl. Geophys. **58**, 157 (1964).
[14] F. Ward, Astrophys. J. **141**, 534 (1965).